Supplement of The Cryosphere, 13, 1819–1842, 2019
https://doi.org/10.5194/tc-13-1819-2019-supplement

The Cryosphere Open Access EGU

Supplement of

Development of physically based liquid water schemes for Greenland firn-densification models

Vincent Verjans et al.

Correspondence to: Vincent Verjans (v.verjans@lancaster.ac.uk)

S1 Regional Climate Model performance

The climatic forcing (temperature, melt, snowfall, rain and sublimation) is provided by the 5.5 km resolution RACMO2.3p2 regional climate model. Table S1 provides summary statistics of model performance with respect to weather station data from the Institute for Marine and Atmospheric research at Utrecht University (IMAU), from the Programme for Monitoring of the Greenland Ice Sheet (PROMICE) (van As et al., 2016) and from the Greenland Climate Network GC-Net (Steffen et al., 1996). Detailed pointwise comparisons between modelled and observed values of temperature, melt rate and precipitation rate are shown in Figs. S1, S2 and S3. In general, RACMO reaches good agreement the with observed data, and root mean squared errors (RMSE) for daily 2 m height temperatures, annual melt rates and annual precipitation rates are of the order of 5 K, 0.1 m w.e. yr^{-1} and 0.15 m w.e. yr^{-1} respectively. At both FA13 and KAN-U, modelled temperatures and melt rates show very low bias (smaller than 1 K and 0.06 m w.e. yr^{-1}). The low RMSE in melt rates (0.11 and 0.08 m w.e. yr^{-1} respectively) is noteworthy because the total melt rates are large. We note that no precipitation data is available at these sites and only two years of melt data for FA13, but RACMO2.3p2 has shown great agreement with other surface mass balance measurements, especially in accumulation areas (RMSE of 0.08 m w.e. yr^{-1}), although weather stations remain sparse on the GrIS (Noël et al., 2018). There is no evidence that the climatic forcing is a source for bias in the firn models' simulations at these sites.

At the stations of DYE-2 and NASA-SE, observed GC-Net data is of lower quality, which partly explains their relatively larger RMSE in temperature and melt rates. At DYE-2, RMSE in precipitation is still low (0.09 m w.e. yr^{-1}) and the bias is only slightly positive (0.04 m w.e. yr^{-1}). Melt rates tend to be underestimated but the RMSE is reasonable (0.13 m w.e. yr^{-1}). It is difficult to partition the larger errors in temperature (positive bias of 1.2 K) between model and measurement errors, but no indication of firn temperature overestimation appears in the firn models' simulations. At NASA-SE, we hypothesize that the negative bias in precipitation rates (-0.21 m w.e. yr^{-1}) leads to an underestimation of downward advection of cold snow and partly causes the 10 m temperature overestimation in our simulations. Additionally, the temperature overestimation (bias of 1.5 K) could enhance the problem. The negative bias in melt rates (-0.07 m w.e. yr^{-1}) plays an opposite role by underestimating latent heat release. However, annual melt rates are low and the effects of this underestimation are likely minor.

S2 Model Implementation

The model uses a finite-volume scheme with each layer being an independent volume. We use the general mixed-form Picard iteration scheme to solve the RE, as it has been demonstrated that the mixed form of RE can be efficiently used in finite-difference schemes because of its accuracy and its robustness with respect to mass conservation (Celia et al., 1990). The Picard scheme discretises the model using central finite differences for the space derivative and a backward Euler method for the time derivative. The iterative process calculates the value of the pressure head at each iteration and then adjusts the liquid water content according to the water retention curve, Eq. (12). Hydraulic parameters are updated and iterations are repeated until convergence of the solution is achieved. Boundary conditions are the rate of meltwater input at the surface and a no-flow condition at the bottom. Solving the RE in the firn column presents numerical challenges. We adopt an implementation strategy based on the works of Wever et al. (2014) and D'Amboise et al. (2017) who implemented the RE in the snow models SNOWPACK and CROCUS respectively. Here, we give more details about this methodology.

S2.1 Convergence criteria

For the solution reached by the Picard iteration scheme to be considered convergent, it must fulfil different criteria. The convergence criteria between two successive iterations are defined for the head pressure (ε_h) and liquid water content (ε_θ) values as well as for the mass balance error (ε_{MB}) of individual layers. These three criteria are fixed to 10^{-3} m, 10^{-5} and 10^{-8} m respectively, following Huang et al. (1996) and Wever et al. (2014). For each layer, we select ε_θ or ε_h according to the effective saturation. Huang et al. (1996) showed that using ε_θ allows faster convergence. However, it cannot be used in very saturated layers and thus we apply ε_h for

layers where effective saturation exceeds 0.99, in accordance with Wever et al. (2014). The mass-balance criterion is always applied to every layer, regardless of the saturation.

S2.2 Hydraulic conductivity calculation

As we use a central finite difference approach to compute RE, the fluxes are assumed to occur on the interface between adjacent layers. Incoming and outgoing fluxes are computed and this requires the hydraulic conductivity value to be calculated at the top and bottom of every layer *i* and not at the centre. We use the upstream-weighting technique (Forsyth et al., 1995):

$$K_{i+\frac{1}{2}} = \begin{cases} K_i, \ if \ \frac{\Delta h}{\Delta z} - 1 \leq 0 \\ K_{i+1}, \ if \ \frac{\Delta h}{\Delta z} - 1 > 0 \end{cases} \quad \text{(S1)}$$

The advantage of this formulation over a simple arithmetic mean is that it does not lead to oscillatory solutions, regardless of the mesh size (Forsyth et al., 1995; Szymkiewicz, 2009).

S2.3 Dry layers

For numerical stability, a snow layer cannot be completely dry (i.e. $\theta = 0$). Therefore, two cases must be considered: dry layers and refreezing layers. At the start of the flow routine, all layers are initialised with a very low θ value, θ_{dry}. The value must be sufficiently low to avoid influencing the refreezing process but sufficiently high to lead to a convergent solution (D'Amboise et al., 2017). In this study, the θ_{dry} value is fixed at 10^{-6} as this is a tenth of the ε_θ criterion. This corresponds to a 1 m thick snow layer holding 1 µm of liquid water. When the flow routine is called in the firn model, the water content of every dry layer is thus synthetically raised to θ_{dry}, which corresponds to a pre-wetting. The porosity of ice layers that are at high densities (>900 kg m^{-3}) is thus adjusted in order to raise their water content to θ_{dry} in both domains.

Similarly, there is a risk for θ reaching too-low values when refreezing occurs. Therefore, refreezing is allowed only if the θ value is above 0.01% (Wever et al., 2014). This value is above θ_{dry} to avoid refreezing and corresponding latent heat release of the very low amounts of water resulting from the fluxes between layers that are initialised at θ_{dry}. Only at the last time step of the flow routine is the refreezing process allowed to decrease the volumetric water content until θ_{dry}. After that, the pre-wetting amounts of liquid water are subtracted at the end of the flow routine to maintain the mass conservation property of the firn model. At the end of the flow routine, if all the layers have a water content below 10^{-5}, we consider the firn column to be completely dry again so that the flow routine does not have to be called until the next melt event and computational time is largely saved.

S2.4 Dynamical time step adjustment

The numerical solving of RE uses a dynamically adjusted time step. Certain situations, such as the arrival of the wetting front at a stratigraphic transition, require a very small time step whereas larger time steps can be used in other cases without affecting numerical stability. Thus, the time step is adjusted according to the number of iterations, n_{it}, required to achieve convergence of the solution at the previous time step: decreased for a large number of iterations and increased for few iterations. Also, as in Wever et al. (2014) and D'Amboise et al. (2017), a back step case is used: the calculation is stopped and the time step automatically decreased if the solution fails to converge in 15 iterations or if warning signs of instability appear (positive pressure head values, effective saturation exceeding 1 or differences in successive pressure head values exceeding 10^3 m). The time step is bounded between 10^{-20} s and 900 s. The procedure can be summarised as follows:

$$\Delta t_{RE}^{t} = \begin{cases} 1.25 \, \Delta t_{RE}^{t-1}, \ if \ n_{it} \leq 5 \\ \Delta t_{RE}^{t-1} \quad , \ if \ 5 < n_{it} < 10 \\ 0.5 \, \Delta t_{RE}^{t-1} \ , \ if \ 10 \leq n_{it} \leq 15 \\ back \ step \ , \ if \ n_{it} > 15 \end{cases} \quad \text{(S2)}$$

S2.5 Saturated layers and aquifer treatment

If water reaches an impermeable ice layer, the layer above progressively becomes saturated. This means that its hydraulic conductivity progressively increases. As a consequence, the incoming flow becomes very large whereas the outgoing flow is forced to be zero. To deal with this issue, the layer has to be set impermeable once close to saturation and this process must go on for layers above when these reach saturation in turn. When an aquifer is present at the bottom of the domain, the amount of water is held in memory at the start of the flow routine and the end of the domain is set as the top of the aquifer. All the percolating water reaching the end of the domain is added to the aquifer amount and at the end of the routine, this total amount is redistributed in the bottom layers.

S2.6 Partial RE solving

In order to save computational time, the RE is not necessarily solved for the entire domain. If a significant part of the lowest layers is dry, we do not proceed to the calculations for this lower dry part. Starting from the surface, we look for the lowest layer where the water content is at least ε_θ + 0.01 % (above the minimum water content after refreezing). Then we take as lower limit for the RE calculation the layer situated 50 cm below this lowest wet layer. This is recalculated at every time step of the RE solving, making the 50 cm addition largely sufficient to capture the wetting of the dry lower part. If the lowest wet layer is less than 50 cm above the end of the domain, then the RE is calculated on the entire domain. This is applied in both the matrix and the preferential flow domains.

S2.7 Refreezing in the preferential flow domain

Contrarily to the SNOWPACK model, there is a particular circumstance for which we apply refreezing directly in the preferential flow domain: if a cold front (subfreezing temperatures) propagates from the surface into a wet firn column, all the water present in the matrix flow domain will progressively be refrozen, starting from the surface layer. It would be unrealistic to keep liquid water present in the preferential flow domain of layers that are above this cold front. Thus, if starting from the surface, the entire firn column until a particular layer that holds some liquid water in the preferential flow domain is at subfreezing temperatures, this liquid water is refrozen. In such cases, the firn column is dry in both domains until the depth delimited by the cold front. Simulations without this refreezing implementation reached very similar results but required more computational time.

S2.8 Merging process

The CFM usually considers every accumulation event as a new layer. However, as we use three hourly accumulation forcing, the firn layer could consist of a high number of extremely fine layers. Because the calculation time for the RE is very dependent on the number of distinct layers in the firn column, we chose to merge any layer thinner than 2 cm with the underlying layer. If this was applied to the surface layer, every accumulation event of less than 2 cm snow would be immediately merged with the previous surface layer. In the case where a high number of successive snowfall events would be below the 2 cm threshold, these would all be merged within the same layer, possibly becoming very thick. To avoid this, the newly added snow layer is merged with the previous surface layer only if the latter is below the 2 cm threshold. However, newly-added layers that are less than 0.01 mm thick are always merged with the layer below. It is important to keep a high vertical resolution when simulating the percolation process with the RE, as this flow equation is highly sensitive to structural heterogeneities in the firn. If the merging process is too lenient, this leads to the smoothing of heterogeneities such as sharp grain-size or density transitions. Moreover, using a coarse resolution would lead to only an approximation of the water percolation because water content is always homogeneous in a single layer. Thus, as soon as water percolates at the top of a given layer, it is distributed in the entire layer.

Tables

RACMO2.3p2 vs. AWS			Temperature 2 m [K]			Melt [m w.e. yr^{-1}]			Precipitation [m w.e. yr^{-1}]		
Station	Period	number of observations	R^2	Bias	RMSE	R^2	Bias	RMSE	R^2	Bias	RMSE
NASA-SE	1998-2015	6209	0.61	1.47	6.94	0.77	$-68.34\ 10^{-3}$	$84.48\ 10^{-3}$	0.85	$-206.1\ 10^{-3}$	$228.8\ 10^{-3}$
DYE-2	1998-2015	6209	0.60	1.19	7.32	0.88	$-101.4\ 10^{-3}$	$128.2\ 10^{-3}$	0.78	$43.58\ 10^{-3}$	$90.30\ 10^{-3}$
KAN-U	2009-2016	2718	0.97	0.88	2.09	0.93	$14.00\ 10^{-3}$	$81.92\ 10^{-3}$	-	-	-
FA13	2014-2016	352	0.92	0.87	2.20	-	$-51.56\ 10^{-3}$	$105.8\ 10^{-3}$	-	-	-

Table S1. Statistics of comparison between RACMO2.3p2 climatic output and Automatic Weather Station measurements, hyphens indicate absence or paucity of data

Variable/Parameter	Symbol	Value [unit]
Density	ρ	[kg m^{-3}]
Ice density	ρ_i	917 [kg m^{-3}]
Water density	ρ_w	1000 [kg m^{-3}]
Temperature	T	[K]
Mean annual surface temperature	T_{av}	[K]
Mean annual accumulation rate	$\dot{b}$	[m s^{-1}]
Gas constant	R	8.314 [J mol^{-1} K^{-1}]
Gravitational acceleration	g	9.81 [m s^{-2}]
Overburden pressure	σ	[kg m^{-1} s^{-2}]
Snow viscosity	η	[kg m^{-1} s^{-1}]
Firn viscosity parameters	η_0	7.62237 [kg s^{-1} m^{-1}]
	a_n	0.1 [K^{-1}]
	b_n	0.023 [m^3 kg^{-1}]
	c_n	358 [kg m^{-3}]
	f_1	4 [/]
	f_2	[/]
Firn thermal conductivity	k_s	[W m^{-1} K^{-1}]
Pressure head	h	[m]
Hydraulic conductivity	$K(\theta)$	[m s^{-1}]
Hydraulic conductivity at saturation	$Ksat$	[m s^{-1}]
Grain radius	r	[m]
Grain radius at surface	r_0	[m]
Grain growth activation energy	E_g	42.4 10^3 [J mol^{-1}]
Grain growth rate constant	k_g	1.3 10^{-7} [m^2 s^{-1}]
Initial grain-size parameters	b_0	0.781 [/]
	b_1	0.0085 [/]
	b_2	-0.279 [/]
Dynamic viscosity of liquid water at 273.15 K	μ	0.001792 [kg m^{-1} s^{-1}]
Volumetric water content	θ	[/]
Water-holding capacity	θ_h	[/]
Mass proportion corresponding to water-holding capacity	W_w	[/]
Residual water content	θ_r	[/]
Porosity	P	[/]
Fraction of the pore space allocated to preferential flow	F	0.02 [/]
Saturated water content	θ_{sat}	[/]
Effective saturation	Se	[/]
van Genuchten parameters	α, n, m	[/]
Water entry suction	h_{we}	[m]
Heat flow	Q	[J m^{-2} s^{-1}]
Specific latent heat of fusion	L_f	[J kg^{-1}]
Concentration of preferential flowpaths	N	[m^{-2}]

Preferential flow saturation threshold	Θ	0.1 [/]
Lateral runoff	Ru	[m]
Water in excess of the residual water content	L_{excess}	[m]
Characteristic runoff time	τ_{Ru}	[s]
Surface slope	S	[/]
Runoff parameters	c_1	$1.296\ 10^5$ [s]
	c_2	$2.16\ 10^6$ [s]
	c_3	140 [/]
Mass liquid water content	$\theta_{weight,\%}$	[%]
Correction factor in water-retention curve	Sc	$[1 + (0.0058\alpha)^n]^{-m}$ [/]

Table S2. Variables and parameters notation

Liquid water scheme [Abbreviation]	Bucket model [BK]; Single-domain Richards Equation [R1M]; Dual-permeability Richards Equation [DPM]
Compaction scheme [Abbreviation]	CROCUS [CR]; Herron and Langway (1980) [HL]; Kuipers Munneke et al. (2015) [KM]
Impermeability threshold [Abbreviation]	780 kg m^{-3} [ip780]; 810 kg m^{-3} [ip810]; 830 kg m^{-3} [ip830]
Water-holding capacity [Abbreviation]	Constant at 2 % [wh02]; Coléou and Lesaffre (1998) [whCL]
Grain-size formulation [Abbreviation]	Linow et al. (2012) at surface and Katsushima et al. (2009) growth [grLK]; Constant at surface and Arthern et al. (2010) growth [grA]

Table S3. Options for simulation experiments and their respective abbreviations

	Liquid water scheme	Compaction scheme	Impermeability threshold	Water-holding capacity	Grain-size formulation
BK (wh02 ip810)	BK	CROCUS	810	0.02	/
R1M (grLK ip810)	R1M	CROCUS	810	/	LK
DPM (grLK ip810)	DPM	CROCUS	810	/	LK
DPM (grLK ip780)	DPM	CROCUS	780	/	LK
DPM (grLK ip830)	DPM	CROCUS	830	/	LK
BK (wh02 ip780)	BK	CROCUS	780	0.02	/
BK (whCL ip810)	BK	CROCUS	810	CL	/
BK (wh02 ip830)	BK	CROCUS	830	0.02	/
R1M (grLK ip830)	R1M	CROCUS	830	/	LK
R1M (grA ip810)	R1M	CROCUS	810	/	A
DPM (grA ip810)	DPM	CROCUS	810	/	A
HL DPM (grLK ip810)	DPM	HL	810	/	LK
KM DPM (grLK ip810)	DPM	KM	810	/	LK
HL R1M (grLK ip810)	R1M	HL	810	/	LK
KM R1M (grLK ip810)	R1M	KM	810	/	LK

Table S4. Details of the acronyms of the simulation experiments presented

	Top 15 m FAC, anomaly vs observations				10 m temperature, anomaly vs observations [K]			
	DYE-2	NASA-SE	KAN-U	FA13	DYE-2	NASA-SE	KAN-U	FA13
BK (wh02 ip810)	-4 %	-3 %	+59 %	-23 %	+0.21	+1.94	-1.73	+0.10
R1M (grLK ip810)	-4 %	-3 %	+50 %	-30 %	-0.40	+1.42	-2.57	-0.71
DPM (grLK ip810)	-16 %	-3 %	-2 %	-30 %	+2.72	+2.21	+4.52	+1.5
BK (whCL ip810)	+0 %	-2 %	+65 %	-32 %	-1.27	+1.00	-3.43	-0.66
BK (wh2 ip780)	-1 %	-3 %	+67 %	-22 %	+0.01	+1.94	-2.20	-0.52
BK (wh02 ip830)	-5%	-3 %	+47 %	-23 %	+0.31	+1.94	-0.97	+0.32
R1M (grA ip810)	-0 %	-2 %	+66 %	-27%	-1.03	+1.02	-3.25	-1.88
R1M (grLK ip780)	-2 %	-3 %	+61 %	-30 %	-0.34	+1.42	-2.56	-0.72
R1M (grLK ip830)	-2 %	-3 %	+48 %	-31 %	-0.38	+1.42	-2.45	-0.43
DPM (grA ip810)	-16 %	-3 %	-4 %	-32 %	+2.41	+2.14	+4.62	+1.5
DPM (grLK ip780)	-16 %	-3 %	+13 %	-44 %	+2.78	+2.21	+2.97	+1.5
DPM (grLK ip830)	-14 %	-3 %	-11 %	-28 %	+2.73	+2.21	+5.65	+0.48

Table S5. Summary of the results of the three water schemes and their various parameterisations compared to observations

	Top 15 m FAC, anomaly vs observations				10 m temperature, anomaly vs observations [K]			
	DYE-2	NASA-SE	KAN-U	FA13	DYE-2	NASA-SE	KAN-U	FA13
CR R1M (grLK ip810)	-4 %	-3 %	+50 %	-21 %	-0.40	+1.42	-2.57	-0.19
HL R1M (grLK ip810)	-11 %	+17 %	+37 %	-30 %	-0.26	+1.22	-2.32	-0.71
KM R1M (grLK ip810)	-23 %	+8 %	+10 %	-54 %	-0.41	+1.77	-2.84	-0.75

Table S6. Summary of the results of the three densification models compared to observations

Figures

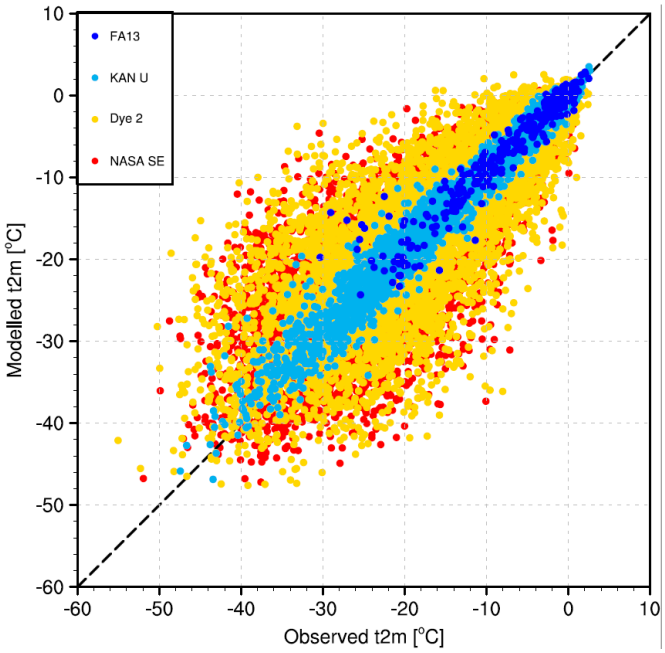

Figure S1. Pointwise comparison between RACMO2.3p2 and Automatic Weather Station data of temperature at 2 m height

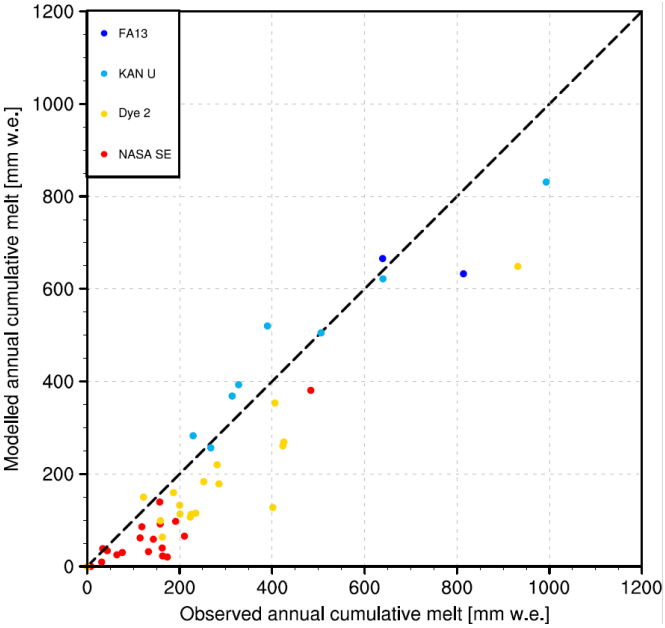

Figure S2. Pointwise comparison between RACMO2.3p2 and Automatic Weather Station data of annual cumulative melt

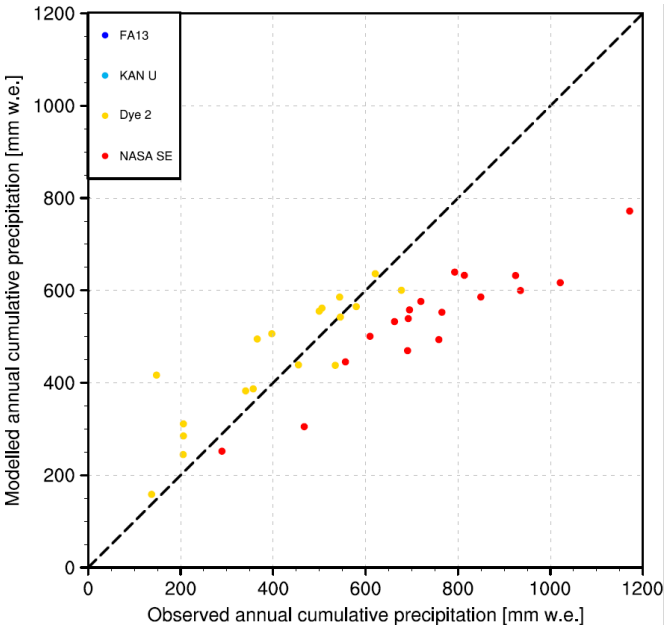

Figure S3. Pointwise comparison between RACMO2.3p2 and Automatic Weather Station data of annual cumulative precipitation

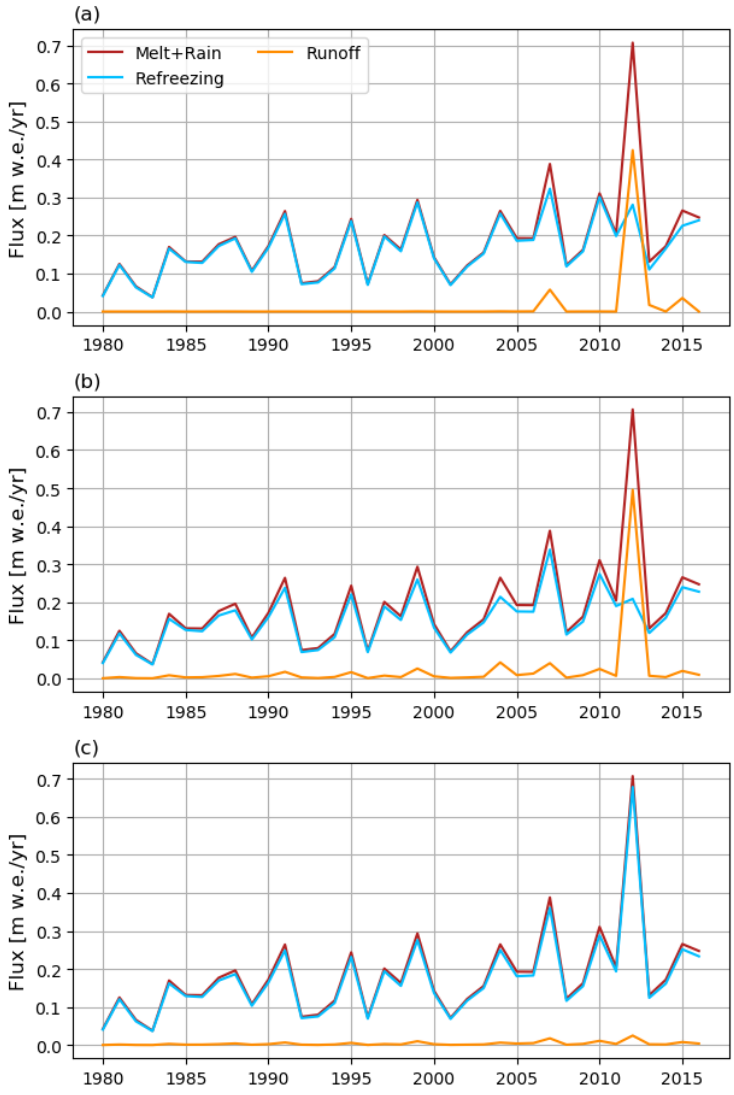

Figure S4. Annual rates of liquid water input, runoff and refreezing at DYE-2 as simulated by (a) BK wh02 ip810, (b) R1M grLK ip810 and (c) DPM grLK ip810

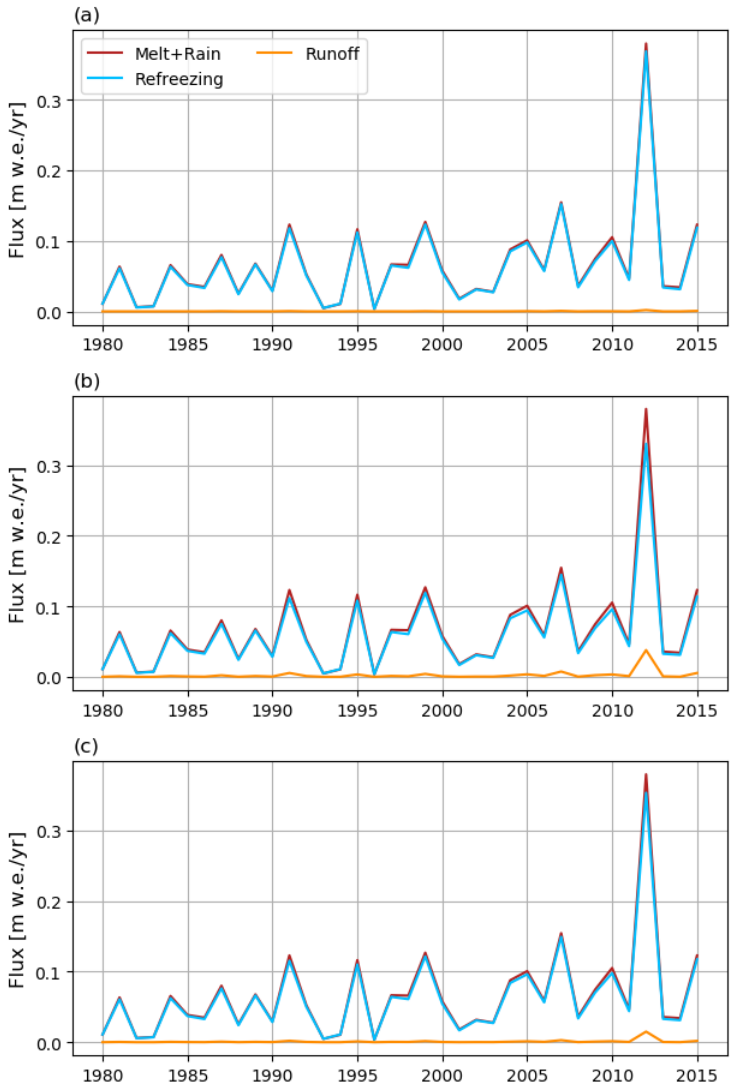

Figure S5. Annual rates of liquid water input, runoff and refreezing at NASA-SE as simulated by (a) BK wh02 ip810, (b) R1M grLK ip810 and (c) DPM grLK ip810

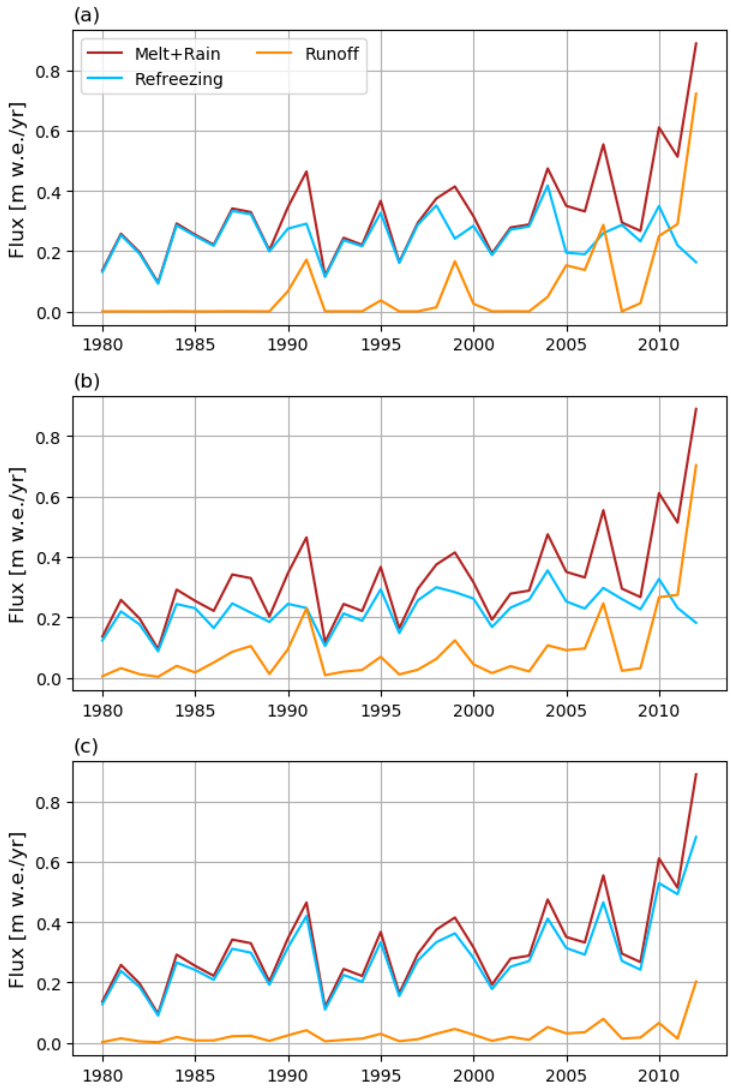

Figure S6. Annual rates of liquid water input, runoff and refreezing at KAN-U as simulated by (a) BK wh02 ip810, (b) R1M grLK ip810 and (c) DPM grLK ip810

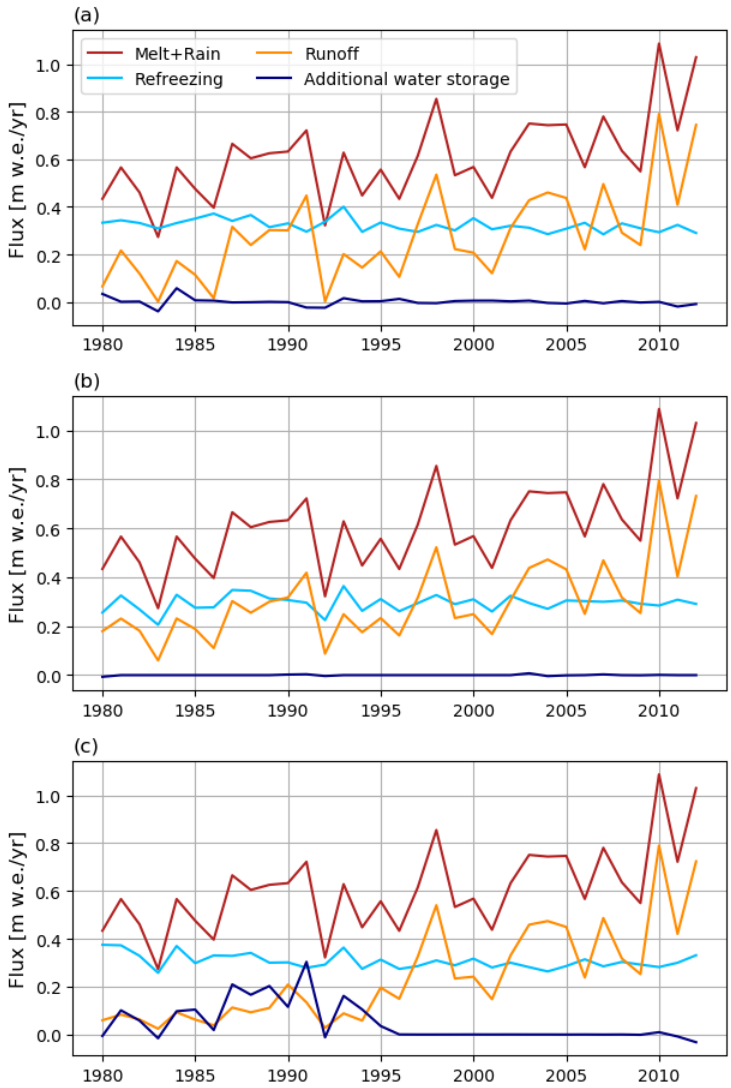

Figure S7. Annual rates of liquid water input, runoff, refreezing and storage of liquid water in the firn column at FA13 as simulated by (a) BK wh02 ip810, (b) R1M grLK ip810 and (c) DPM grLK ip810

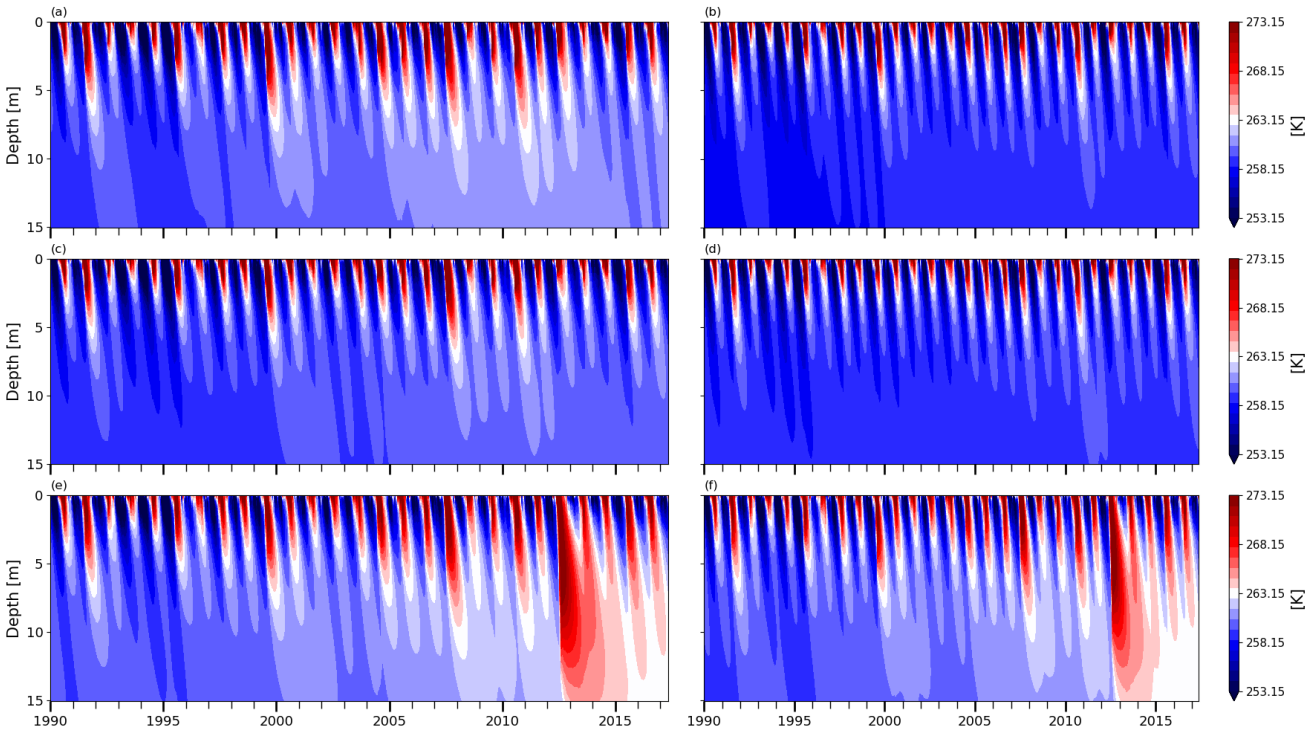

Figure S8. Modelled firn temperature at DYE-2, (a) BK wh02 ip810, (b) R1M grLK ip810, (c) DPM grLK ip810, (d) BK whCL ip810, (e) R1M grA ip810, (f) DPM grA ip810

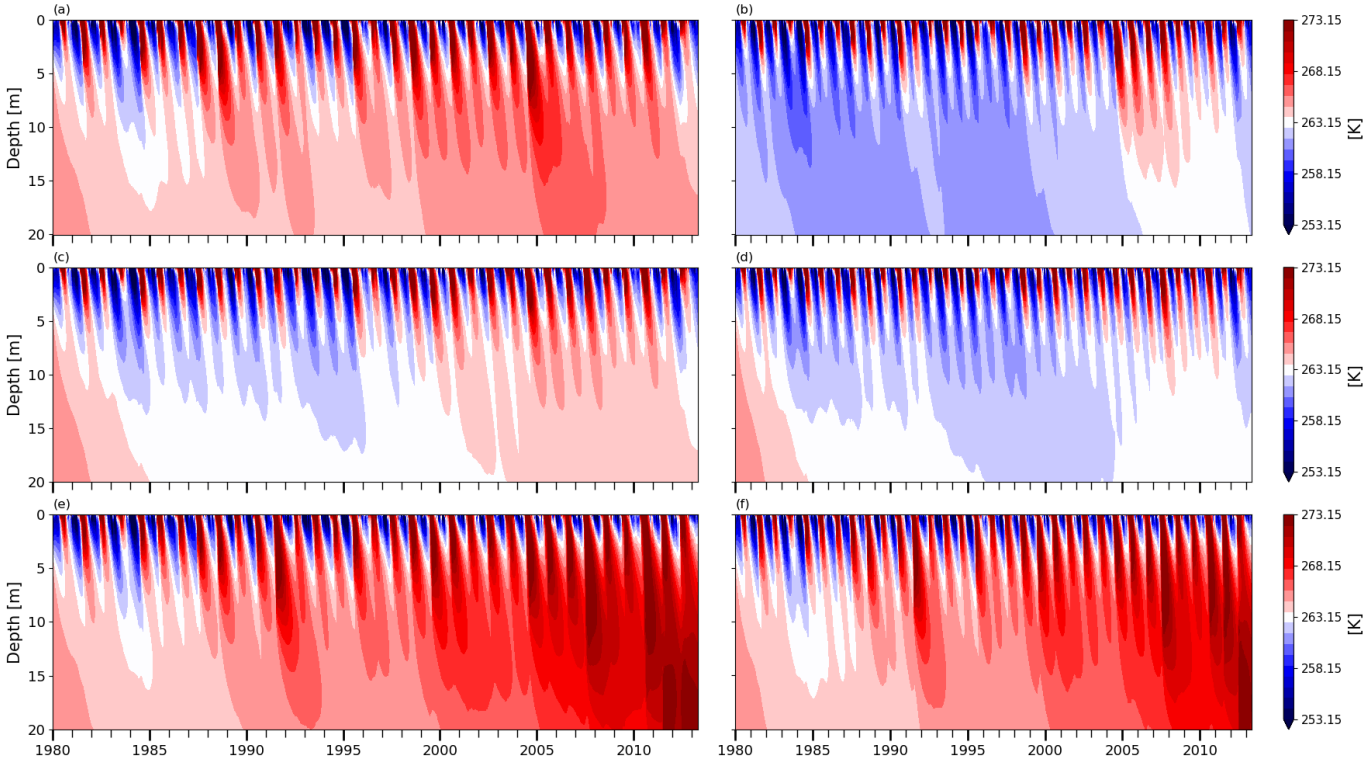

Figure S9. Modelled firn temperature at KAN-U, (a) BK wh02 ip810, (b) R1M grLK ip810, (c) DPM grLK ip810, (d) BK whCL ip810, (e) R1M grA ip810, (f) DPM grA ip810

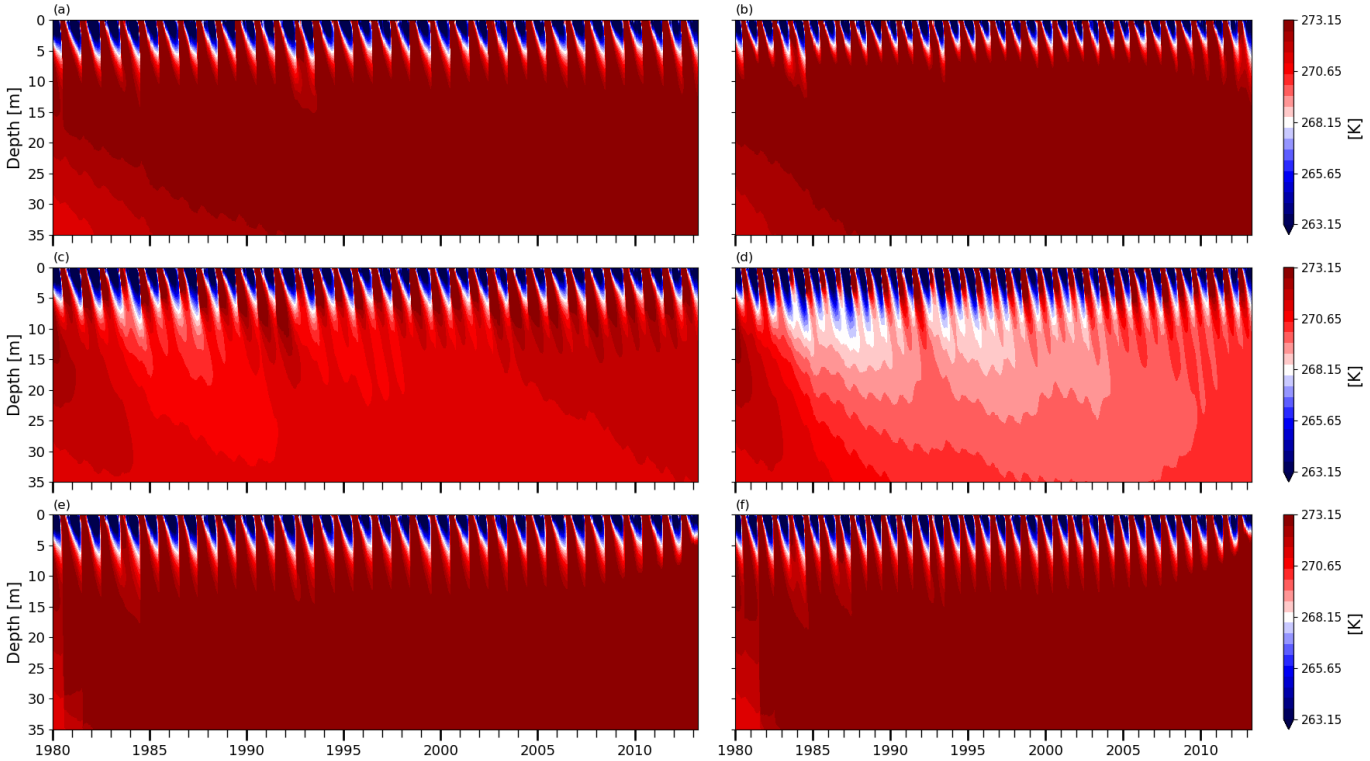

Figure S10. Modelled firn temperature at FA13, (a) BK wh02 ip810, (b) R1M grLK ip810, (c) DPM grLK ip810, (d) BK whCL ip810, (e) R1M grA ip810, (f) DPM grA ip810

References

Arthern, R. J., Vaughan, D. G., Rankin, A. M., Mulvaney, R. and Thomas, E. R.: In situ measurements of Antarctic snow compaction compared with predictions of models, J. Geophys. Res. Earth Surf., 115, 1–12, doi:10.1029/2009JF001306, 2010.

Celia, M. A., Bouloutas, E. T. and Zarba, R. L.: A General Mass-Conservative Numerical Solution for the Unsaturated Flow Equation, Water Resour. Res., 26, 1483–1496, doi:10.1029/90wr00196, 1990.

D'Amboise, C. J. L., Müller, K., Oxarango, L., Morin, S. and Schuler, T. V.: Implementation of a physically based water percolation routine in the CROCUS (V7) snowpack model, Geosci. Model Dev. Discuss., 1–32, doi:10.5194/gmd-2017-56, 2017.

Forsyth, P. A., Wu, Y. S. and Pruess, K.: Robust numerical methods for saturated-unsaturated flow with dry initial conditions in heterogeneous media, Adv. Water Resour., 18, 25–38, doi:10.1016/0309-1708(95)00020-J, 1995.

Herron, M. and Langway, C.: Firn densification: an empirical model, J. Glaciol., 25, 1980.

Huang, K., Mohanty, B. P. and van Genuchten, M. T.: Method To Solve the Variably Saturated Flow Equation, J. Hydrol., 178, 69–91, 1996.

Katsushima, T., Kumakura, T. and Takeuchi, Y.: A multiple snow layer model including a parameterization of vertical water channel process in snowpack, Cold Reg. Sci. Technol., 59, 143–151, doi:10.1016/j.coldregions.2009.09.002, 2009.

Kuipers Munneke, P., Ligtenberg, S. R. M., Noël, B. P. Y., Howat, I. M., Box, J. E., Mosley-Thompson, E., McConnell, J. R., Steffen, K., Harper, J. T., Das, S. B. and van den Broeke, M. R.: Elevation change of the Greenland ice sheet due to surface mass balance and firn processes, 1960-2013, The Cryosphere, 9, 3541–3580, doi:10.5194/tcd-9-3541-2015, 2015.

Linow, S., Hörhold, M. W. and Freitag, J.: Grain-size evolution of polar firn: A new empirical grain growth parameterization based on X-ray microcomputer tomography measurements, J. Glaciol., 58, 1245–1252, doi:10.3189/2012JoG11J256, 2012.

Machguth, H., Macferrin, M., van As, D., Box, J. E., Charalampidis, C., Colgan, W., Fausto, R. S., Meijer, H. A. J., Mosley-Thompson, E. and van de Wal, R. S. W.: Greenland meltwater storage in firn limited by near-surface ice formation, Nat. Clim. Chang., 6, 390–393, doi:10.1038/nclimate2899, 2016.

Marchenko, S., Pohjola, V., Pettersson, R., van Pelt, W. J. J., Vega, C., Machguth, H., BØggild, C. E. and Isaksson, E.: A plot-scale study of firn stratigraphy at Lomonosovfonna, Svalbard, using ice cores, borehole video and GPR surveys in 2012–14, J. Glaciol., 63(237), 67–78, doi:10.1017/jog.2016.118, 2017.

Noël, B., van de Berg, W. J., van Wessem, J. M., van Meijgaard, E. and van As, D.: Modelling the climate and surface mass balance of polar ice sheets using RACMO2 – Part 1 : Greenland (1958 – 2016), The Cryosphere., 811–831, 2018.

Steffen, K., Box, J. E. and Abdalati, W.: Greenland Climate Network: GC-Net, in Glaciers, Ice Sheets and Volcanoes: A Tribute to Mark F. Meier, vol. Report 96-27, pp. 98–103, Cold Regions Research and Engineering Laboratory, Hanover, NH., 1996.

Szymkiewicz, A.: Approximation of internodal conductivities in numerical simulation of one-dimensional infiltration, drainage, and capillary rise in unsaturated soils, Water Resour. Res., 45, 1–16, doi:10.1029/2008WR007654, 2009.

van As, D., Fausto, R. S., Cappelen, J., Van De Wal, R. S. W., Braithwaite, R. J., Machguth, H., Charalampidis, C., Box, J. E., Solgaard, A. M., Ahlstrom, A. P., Haubner, K., Citterio, M. and Andersen, S. B.: Placing Greenland ice sheet ablation measurements in a multi-decadal context, Geol. Surv. Denmark Greenl. Bull., 35, 71–74, 2016.

Wever, N., Fierz, C., Mitterer, C., Hirashima, H. and Lehning, M.: Solving Richards Equation for snow improves snowpack meltwater runoff estimations in detailed multi-layer snowpack model, The Cryosphere, 8, 257–274, doi:10.5194/tc-8-257-2014, 2014.